Control and optimization for non-local and fractional differential equations

Umberto Biccari and Enrique Zuazua

Chair of Computational Mathematics, Bilbao, Basque Country, Spain

Chair for Dynamics, Control and Numerics, Friedrich-Alexander-Universität Erlangen-Nürnberg, Germany.

Universidad Autónoma de Madrid, Spain.

umberto.biccari@deusto.es enrique.zuazua@fau.de

cmc.deusto.es dcn.nat.fau.eu

PART IV: numerical approximation of differential equations and numerical control

LECTURE 13: numerical approximation and control of waves

Introduction

Introduction

We analyze propagation properties of numerical waves obtained through a finite difference discretization on uniform or non-uniform meshes.

Our approach is based on the study of the propagation of high-frequency Gaussian beam solutions.

Seminal idea

The energy of Gaussian beam solutions propagates along bi-characteristic rays, which are obtained from the Hamiltonian system associated to the symbol of the operator under consideration.

- **CONTINUOUS SETTING:** these techniques date back to Hörmander, and they have been extended by several authors (Gérard, Tartar, Wigner).
- **DISCRETE SETTING:** extension of micro-local techniques to the study of the propagation properties for discrete waves (Maciá, Marica, Zuazua).

A. Marica and E. Zuazua, *Propagation of 1d waves in regular discrete heterogeneous media: a Wigner measure approach*, Found. Comp. Math., 2015.

U. Biccari, A. Marica and E. Zuazua, *Propagation of one- and two-dimensional discrete waves under finite difference approximation*, Found. Comp. Math., 2020.

Gaussian beams

$$\begin{cases} \rho(x)\partial_t^2 u(x,t) - div\big(\sigma(x)\nabla u(x,t)\big) = 0, & (x,t) \in \mathbb{R}^N \times (0,T) \\ u(x,0) = u^0(x), \quad \partial_t u(x,0) = u^1(x), & x \in \mathbb{R}^N \end{cases} \tag{1}$$

PRINCIPAL SYMBOL: $\mathcal{H}(x,t,\xi,\tau) = -\rho(x)\tau^2 + \sigma(x)|\xi|^2$

BI-CHARACTERISTIC RAYS: solutions to the first order ODE system

$$\begin{cases} \dot{x}(s) = \nabla_\xi \mathcal{H}(x(s),t(s),\xi(s),\tau(s)), & x(0) = x_0 \\ \dot{t}(s) = \partial_\tau \mathcal{H}(x(s),t(s),\xi(s),\tau(s)), & t(0) = 0 \\ \dot{\xi}(s) = -\nabla_x \mathcal{H}(x(s),t(s),\xi(s),\tau(s)), & \xi(0) = \xi_0 \\ \dot{\tau}(s) = -\partial_t \mathcal{H}(x(s),t(s),\xi(s),\tau(s)), & \tau(0) = \tau_0 \ \ s.t. \ \ \mathcal{H}(x_0,0,\xi_0,\tau_0) = 0. \end{cases}$$

Rays of geometric optics

$(t, x(t))$: projection of a bi-characteristic to the physical time-space domain.

Gaussian beams

Gaussian beams (GB) expansion

$$u^\varepsilon(x,t) = \varepsilon^{1-\frac{N}{4}} a(x,t) e^{\frac{i}{\varepsilon}\phi(x,t)}$$

$$\phi(x,t) = \xi(t)(x-x(t)) + \frac{1}{2}(x-x(t))^T M(t)(x-x(t)), \quad \Im(M(t)) > 0$$

1. u^ε is an approximate solution of the wave equation (1):
$$\sup_{t\in(0,T)} \|\Box u^\varepsilon(\cdot,t)\|_{L^2(R^N_x)} \leq C\varepsilon^{\frac{1}{2}}.$$
2. The energy of u^ε is bounded with respect to ε.
3. The energy of u^ε is exponentially small off the ray $(x(t),t)$:
$$\sup_{t\in(0,T)} \int_{\mathbb{R}^N\setminus B(t)} |\rho u_t^\varepsilon|^2 + |\sigma\nabla u^\varepsilon|^2\, dx \leq Ce^{-\beta/\sqrt{\varepsilon}}$$
$$\beta > 0,\ B(t) := B(x(t), \varepsilon^{\frac{1}{4}})$$

J. Ralston, Studies in Partial Differential Equations, 1982

F. Maciá and E. Zuazua, Asymptot. Anal., 2002

J. Rauch, X. Zhang and E. Zuazua, J. Math. Pures Appl., 2005

Finite difference wave propagation

We address the problem on three levels:

- The **one-dimensional** wave equation with **constant** coefficients:

$$\partial_t^2 u - \partial_x^2 u = 0, \quad (x,t) \in (-1,1) \times (0,T);$$

- The **one-dimensional** wave equation with **variable** coefficients:

$$\rho(x)\partial_t^2 u - \partial_x(\sigma(x)\partial_x u) = 0, \quad (x,t) \in (-1,1) \times (0,T);$$

- The **two-dimensional** wave equation:

$$\rho(x,y)\partial_t^2 u - div(\sigma(x,y)\nabla u) = 0, \quad (x,y,t) \in (-1,1)^2 \times (0,T).$$

In all cases we will consider zero Dirichlet boundary condition.

Our principal aim is to illustrate that numerical high-frequency solutions can behave in unexpected manners, as a result of the accumulation of the local effects introduced by the heterogeneity of the numerical grid.

One-dimensional wave equation

Semi-discrete approximation

Uniform mesh

$$\mathcal{G}^h := \left\{ x_j := -1 + jh, j = 0, \dots, N+1 h = 2/(N+1),\ N \in \mathbb{N}^* \right\}$$

Non-uniform mesh

- $g \in C^2(\mathbb{R})$
- $0 < g_d^- \leq |g'(x)| \leq g_d^+ < +\infty$
- $|g''(x)| \leq g_{dd} < +\infty$

$$\Longrightarrow \quad \mathcal{G}_g^h := \left\{ g_j := g(x_j),\ x_j \in \mathcal{G}^h \right\}$$

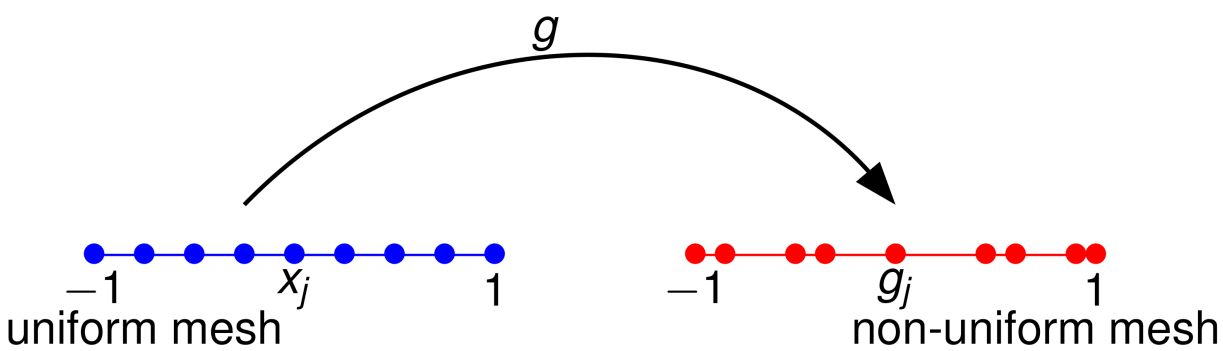

Semi-discrete approximation

- $h_{j+1/2} := g_{j+1} - g_j, \quad j = 0, \dots, N$
- $h_{j-1/2} := g_j - g_{j-1}, \quad j = 1, \dots, N+1$
- $h_j := \frac{h_{j+1/2} + h_{j-1/2}}{2}, \quad j = 1, \dots, N$

Semi-discrete wave equation

$$\begin{cases} h_j u_j''(t) - \left(\dfrac{u_{j+1}(t) - u_j(t)}{h_{j+1/2}} - \dfrac{u_j(t) - u_{j-1}(t)}{h_{j-1/2}} \right) = 0 \\ u_0(t) = u_{N+1}(t) = 0 \\ u_j(0) = u_j^0, \quad u_j'(0) = u_j^1 \\ j = 1, \dots, N, \quad t \in (0, T). \end{cases}$$

Hamiltonian system

Hamiltonian

$$\mathcal{H}_c(x,t,\xi,\tau) = -\tau^2 + \xi^2$$

Bi-characteristic rays

$$\begin{cases} \dot{x}(s) = 2\xi(s), & x(0) = x_0 \\ \dot{t}(s) = -2\tau(s), & t(0) = 0 \\ \dot{\xi}(s) = 0, & \xi(0) = \xi_0 \\ \dot{\tau}(s) = 0, & \tau(0) = \tau_0 \end{cases} \quad s.t. \quad \mathcal{H}_c(x_0, 0, \xi_0, \tau_0) = 0.$$

- For any ξ_0 there are two characteristics starting from x_0: $x^{\pm}(t) = x_0 \mp t$.
- Each one of these characteristics reaches the boundary of $(-1,1)$ in a uniform time and reflects according to the geometric optics laws.

Discrete Hamiltonian system

Discrete Hamiltonian

$$\mathcal{H}(y,t,\xi,\tau) := -\tau^2 + c_g(y)^2\omega(\xi)^2$$

$$y = g^{-1}(x), \quad c_g(y) := \frac{1}{g'(y)}, \quad \omega(\xi) := 2\sin\left(\frac{\xi}{2}\right)$$

Discrete bi-characteristic rays

$$\begin{cases} \dot{y}(s) = 2c_g(y(s))^2\omega(\xi(s))\partial_\xi\omega(\xi(s)), & y(0) = y_0 \\ \dot{t}(s) = -2\tau(s), & t(0) = 0 \\ \dot{\xi}(s) = -2c_g(y(s))\partial_y c_g(y(s))\omega(\xi(s))^2, & \xi(0) = \xi_0 \\ \dot{\tau}(s) = 0, & \tau(0) = \tau_0 \end{cases}$$

- $\partial_\xi\omega(\xi)$: **group velocity**, i.e. the speed at which the energy associated with wave number ξ moves.

Discrete Hamiltonian system

- $\forall s,\ \tau(s) = \tau_0$
- $H(y(s), t(s), \xi(s), \tau(s)) = 0$

$$\Rightarrow \quad \boxed{\tau_0^{\pm} = \pm c_g(y(s))|\omega(\xi(s))|}$$

Since $\dot{t}(s) \neq 0$, the Inverse Function Theorem allows to parametrize the curve $s \mapsto (y(s), t(s), \xi(s), \tau_0^{\pm})$ by $t \mapsto (y(t), t, \xi(t), \tau_0^{\pm})$.

$$\begin{cases} \dot{y}^{\pm}(t) = \mp c_g(y^{\pm}(t))\partial_\xi \omega(\xi^{\pm}(t)) \\ \dot{\xi}^{\pm}(t) = \pm \partial_y c_g(y^{\pm}(t))\omega(\xi^{\pm}(t)) \\ y^{\pm}(0) = y_0, \quad \xi^{\pm}(0) = \xi_0 \end{cases}$$

- $c_g(\cdot) > 0$

$$\Rightarrow \quad \boxed{|\dot{y}^{\pm}(t)| = c_g(y^{\pm}(t))\left|\partial_\xi \omega(\xi^{\pm}(t))\right|}$$

- The velocity of the rays vanishes if, and only if, $\partial_\xi(\omega) = \cos(\xi/2) = 0$, i.e. $\xi = (2k+1)\pi$, $k \in \mathbb{Z}$.
- When $\omega(\xi) = \xi$, corresponding to the continuous case, this cannot happen.

Numerical results

- $\mathbf{x}^h$: uniform mesh of size $h = 2/(N+1)$.
- $\mathbf{g}^{h,1} := \tan\left(\frac{\pi}{4}\mathbf{x}^h\right)$ and $\mathbf{g}^{h,2} := 2\sin\left(\frac{\pi}{6}\mathbf{x}^h\right)$: non-uniform grids

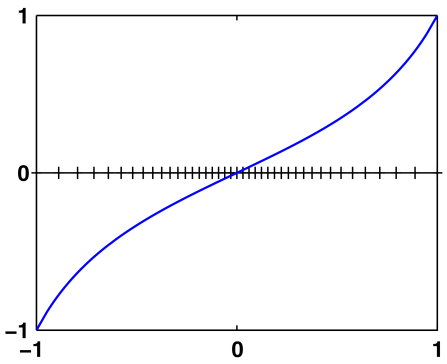

$\mathbf{g}^{h,1}$

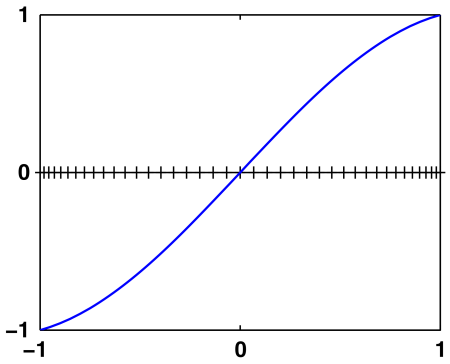

$\mathbf{g}^{h,2}$

Time discretization: **leap-frog scheme** with CFL condition $\delta t = 0.1 \cdot h$

Initial data built from a Gaussian profile:

$$G_\gamma(x) = e^{-\frac{\gamma}{2}\left(g^{-1}(x)-g^{-1}(x_0)\right)^2} e^{i\frac{\xi_0}{h}g^{-1}(x)}, \quad u^0(x) = G_\gamma(x), \quad u^1(x) = (u^0)'(x).$$

Hamiltonian system

Hamiltonian system in the x variable

$$\begin{cases} \dot{x}^{\pm}(t) = \mp a_g(x^{\pm}(t)) \cos\left(\dfrac{\xi^{\pm}(t)}{2}\right), & x^{\pm}(0) = x_0 \\ \dot{\xi}^{\pm}(t) = \pm 2 b_g(x^{\pm}(t)) \sin\left(\dfrac{\xi^{\pm}(t)}{2}\right), & \xi^{\pm}(0) = \xi_0. \end{cases}$$

$$a_g(\cdot) := (g' c_g)(g^{-1}(\cdot)),\ b_g(\cdot) := c_g'(g^{-1}(\cdot)),\ x_0 = g(y_0).$$

- Independently of the choice of the function g, we always have $a_g \equiv 1$.
- For each mesh refinement, b_g can be computed explicitly:

▷ $g(y) = \tan\left(\dfrac{\pi}{4} y\right) \quad \Rightarrow \quad b_g(x) = -\dfrac{2x}{x^2+1}$

▷ $g(y) = 2\sin\left(\dfrac{\pi}{6} y\right) \quad \Rightarrow \quad b_g(x) = \dfrac{x}{4-x^2}$

Phase portrait

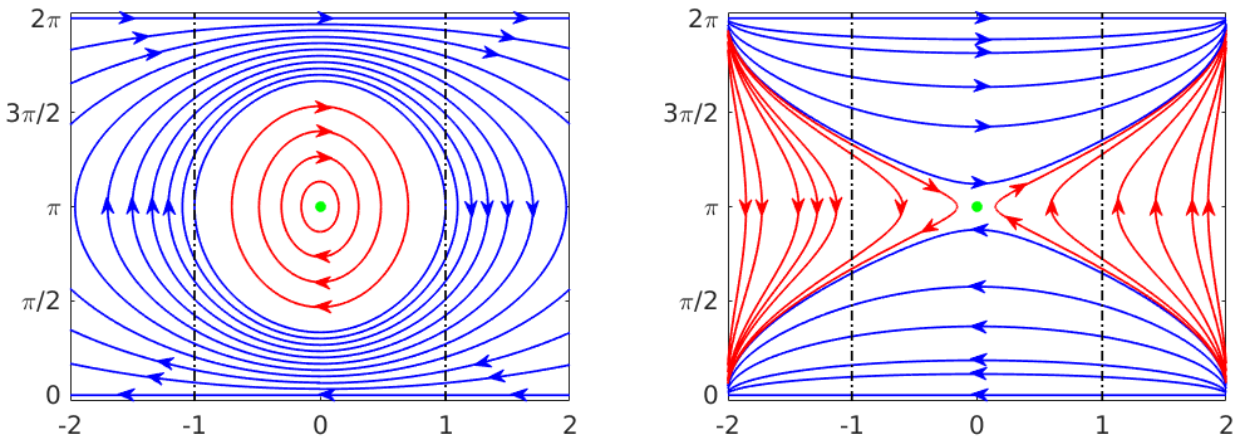

EQUILIBRIUM: $P_e := (x_e, \xi_e) = (0, \pi)$

- tangential mesh (left): **CENTER** (stable equilibrium)
- sinusoidal mesh (right): **SADDLE** (unstable equilibrium)

Plots

At low frequencies, the numerical solutions behave like the continuous ones: they propagate along straight characteristic lines and reflect following the Descartes-Snell's law when they touch one of the two endpoints.

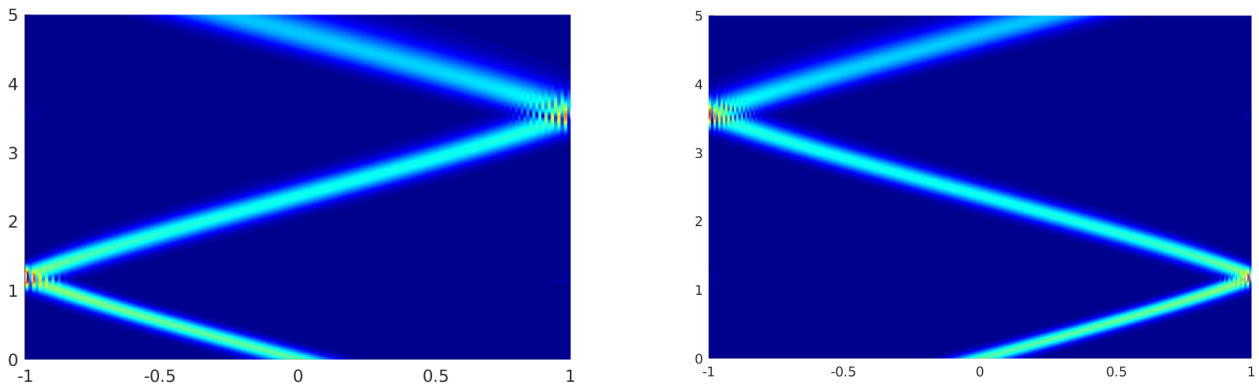

Propagation of a Gaussian wave packet with initial frequency $\xi_0 = \pi/4$ (left) and $\xi_0 = 7\pi/4$ (right), employing the mesh $\mathbf{g}^{h,1}$.

High-frequency pathologies

NON-PROPAGATING WAVES ($x_0 = 0, \xi_0 = \pi$)

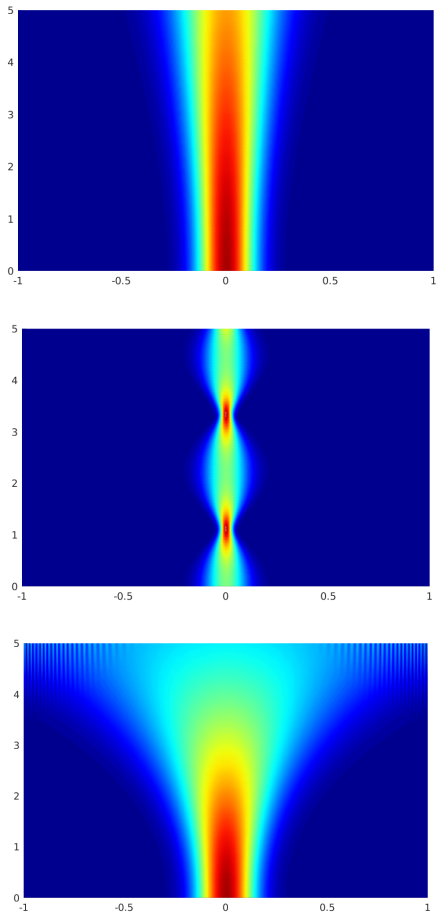

JUSTIFICATION

- The non propagating waves correspond to the equilibrium point P_e on the phase diagram.
- For $\xi = \pi$ we have $\partial_\xi \omega(\xi) = 0$ and, therefore, the velocity of the rays vanishes.

High-frequency pathologies

INTERNAL REFLECTION

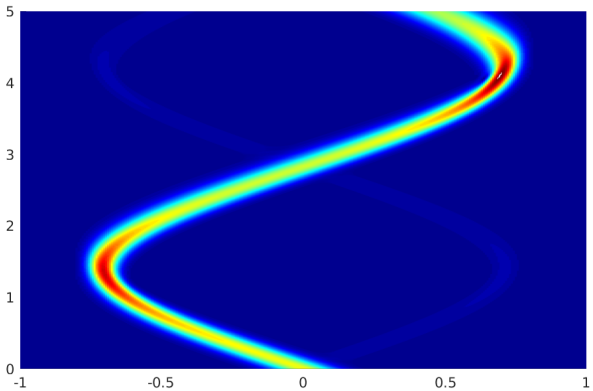

$x_0 = 0, \xi_0 = \frac{7\pi}{15}$, mesh $\mathbf{g}^{\mathbf{h,1}}$

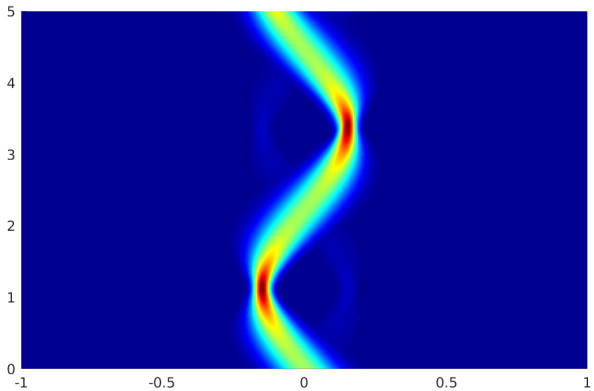

$x_0 = 0, \xi_0 = \frac{13\pi}{15}$, mesh $\mathbf{g}^{\mathbf{h,1}}$

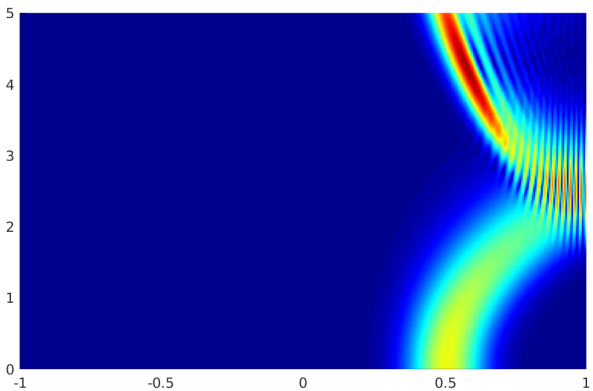

$x_0 = \frac{1}{2}, \xi_0 = \pi$, mesh $\mathbf{g}^{\mathbf{h,2}}$

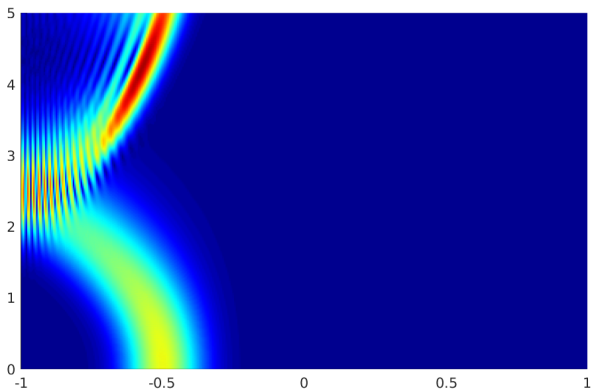

$x_0 = -\frac{1}{2}, \xi_0 = \pi$, mesh $\mathbf{g}^{\mathbf{h,2}}$

High-frequency pathologies

JUSTIFICATION

- On the mesh $\mathbf{g}^{h,1}$, approaching the endpoints of the domain the step size increases and the group velocity $1/h$ of the high-frequency waves decreases. If this group velocity vanishes before the wave has reached the boundary, then this results in a process of internal reflection.
- For the mesh $\mathbf{g}^{h,2}$, P_e is a saddle point, and the red curves always remain trapped either in the region $x \in [0,1]$ or $x \in [-1,0]$.
- The amplitude of the wave is the one of the Gaussian profile of the initial datum, which is of the order of $h^{-0.9}$. On the mesh $\mathbf{g}^{h,1}$, while approaching the boundary h increases. Therefore, the support of the ray shrinks and, due to energy conservation, the high of the corresponding wave has to increase.

Variable coefficients case

Variable coefficients wave equation

$$\begin{cases} \rho(x)\partial_t^2 u - \partial_x(\sigma(x)\partial_x u) = 0, & (x,t) \in (-1,1) \times (0,T) \\ u(-1,t) = u(1,t) = 0, & t \in (0,T) \\ u(x,0) = u^0(x), \quad \partial_t u(x,0) = u^1(x), & x \in (-1,1), \end{cases}$$

$\rho, \sigma \in L^\infty(\mathbb{R})$ with $\rho(x) \geq \rho^* > 0$ and $\sigma(x) \geq \sigma^* > 0$.

PRINCIPAL SYMBOL: $\mathcal{H}_c(x,t,\xi,\tau) = -\rho(x)\tau^2 + \sigma(x)\xi^2$

BI-CHARACTERISTIC RAYS: solutions to the first order ODE system

$$\begin{cases} \dot{x}(s) = 2\sigma(x(s))\xi(s), & x(0) = x_0 \\ \dot{t}(s) = -2\rho(x(s))\tau(s), & t(0) = 0 \\ \dot{\xi}(s) = \rho'(x(s))\tau^2(s) - \sigma'(x(s))\xi^2(s), & \xi(0) = \xi_0 \\ \dot{\tau}(s) = 0, & \tau(0) = \tau_0 \quad s.t. \quad \mathcal{H}_c(x_0,0,\xi_0,\tau_0) = 0. \end{cases}$$

Notice that the bi-characteristics are not straight lines, since $\dot{\xi}(s) \neq 0$.

Discrete Hamiltonian

Uniform mesh

$$\mathcal{H}(y,t,\xi,\tau) := -\tau^2 + c_g(y)^2\omega(\xi)^2$$

$$y = g^{-1}(x), \quad c_g(y) := \frac{1}{g'(y)}\sqrt{\frac{\sigma(g(y))}{\rho(g(y))}}, \quad \omega(\xi) := 2\sin\left(\frac{\xi}{2}\right)$$

Discrete bi-characteristic rays

$$\begin{cases} \dot{y}^{\pm}(t) = \mp c_g(y^{\pm}(t))\partial_\xi\omega(\xi^{\pm}(t)), & y^{\pm}(0) = y_0 \\ \dot{\xi}^{\pm}(t) = \pm\partial_y c_g(y^{\pm}(t))\omega(\xi^{\pm}(t)), & \xi^{\pm}(0) = \xi_0. \end{cases}$$

Numerical results

COEFFICIENTS: $\rho(x) \equiv 1$ and $\sigma(x) = 1 + A\cos^2(\kappa\pi x)$, $A > 0,\ \kappa \in \mathbb{N}^*$.

Hamiltonian system

$$\begin{cases} \dot{x}(t) = -\sqrt{1 + A\cos^2(\kappa\pi x(t))}\cos\left(\dfrac{\xi(t)}{2}\right), & x(0) = x_0 \\ \dot{\xi}(t) = F_j^{A,\kappa}(x(t))\sin\left(\dfrac{\xi(t)}{2}\right), & \xi(0) = \xi_0,\ \ j = 0, 1, 2. \end{cases}$$

- $j = 0$: uniform mesh
- $j = 1$: tangential mesh
- $j = 2$: sinusoidal mesh

Plots

LOW-FREQUENCY SOLUTIONS: $(\xi_0 = \pi/7)$

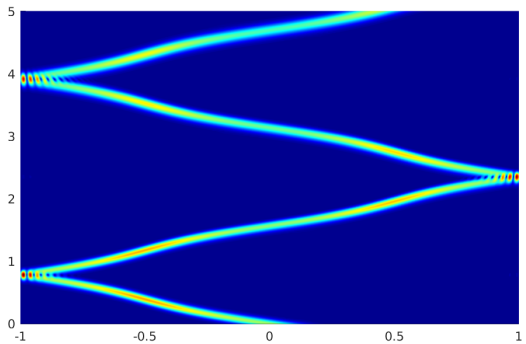

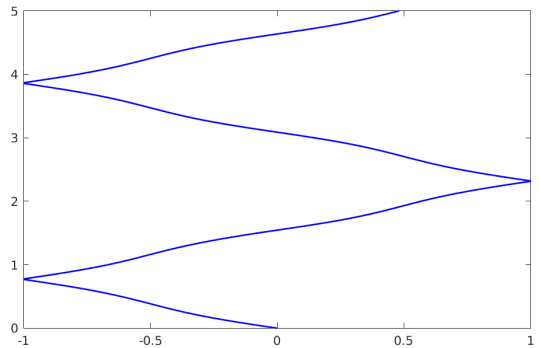

$A = 2, \kappa = 1.$

- The wave travels along characteristics and reaches the boundary, where it is reflected according to the Descartes-Snell's law.
- The parameters A and κ in the coefficient σ affect the shape of the rays.

Plots

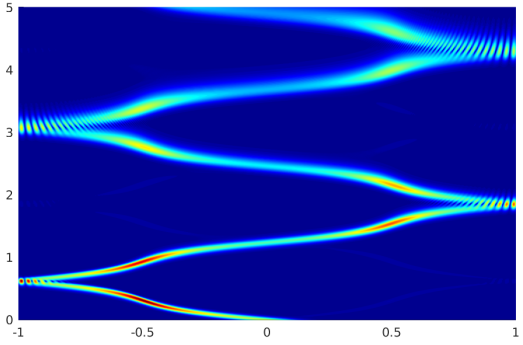

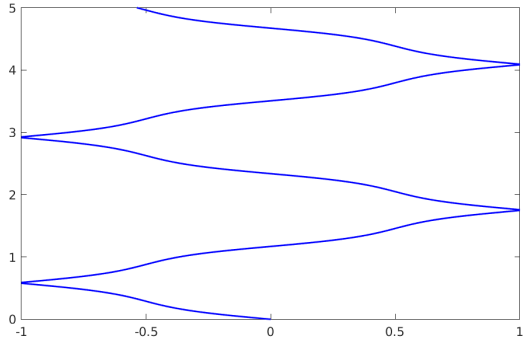

$A = 7$, $\kappa = 1$.

- $A_1 \geq A_2 \quad \Rightarrow \quad |\dot{x}_{A_1,\kappa}(t)| \geq |\dot{x}_{A_2,\kappa}(t)|, \quad |\ddot{x}_{A_1,\kappa}(t)| \geq |\ddot{x}_{A_2,\kappa}(t)|$

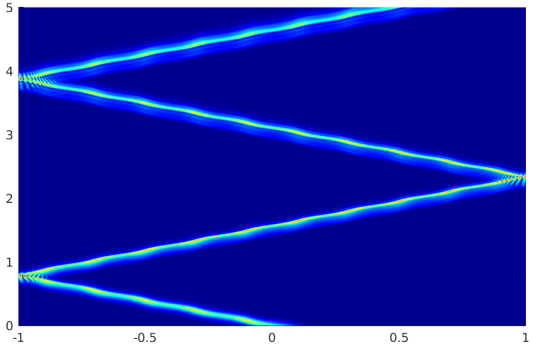

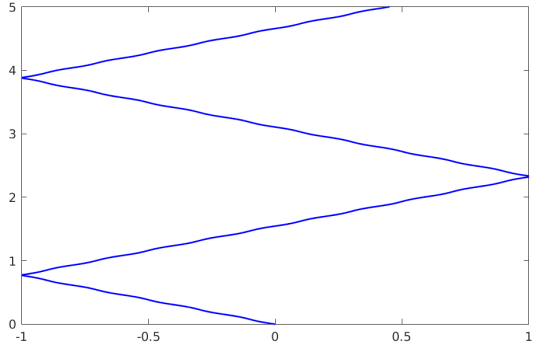

$A = 2$, $\kappa = 5$.

- σ is a periodic function of period $T = 2\kappa$.

High-frequency pathologies

In what follows, we will always assume $A = 1$ and $\kappa = 1$ in the coefficient σ.

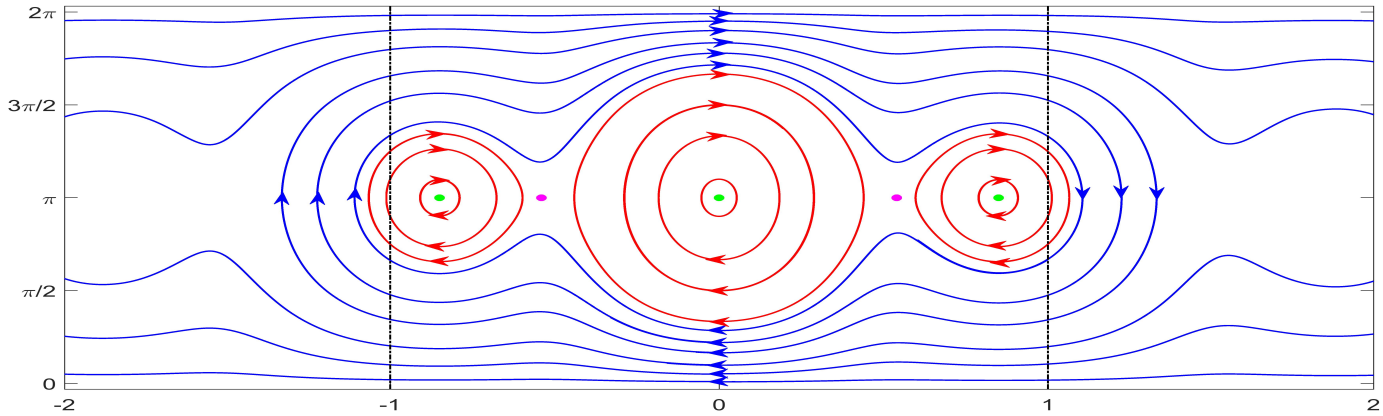

Mesh $\mathbf{g}^{\mathbf{h},\mathbf{1}}$

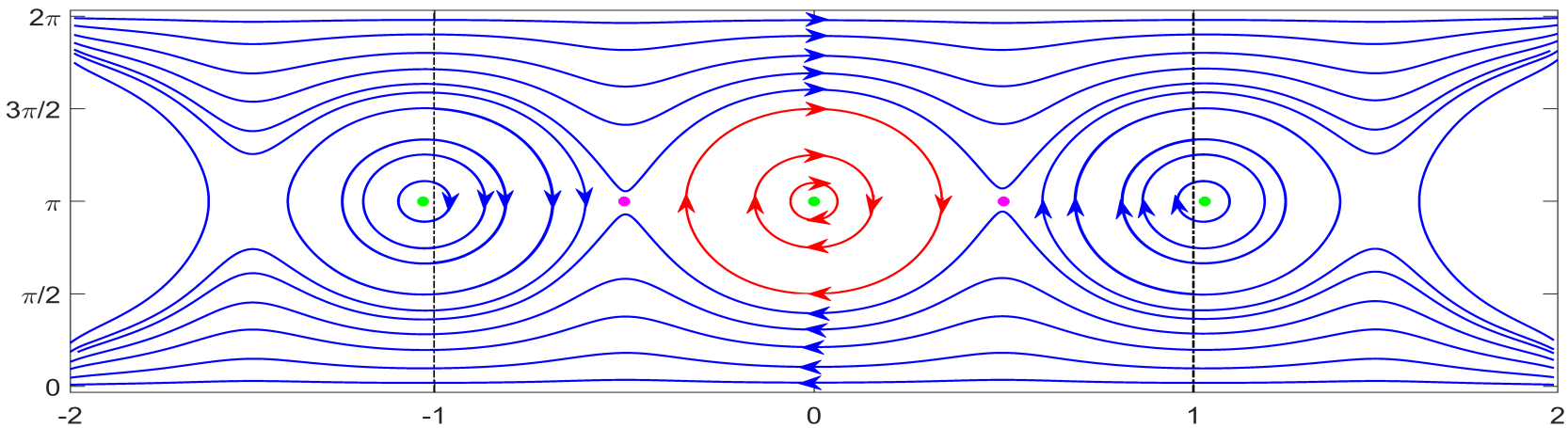

Mesh $\mathbf{g}^{\mathbf{h},\mathbf{2}}$

High-frequency pathologies

NON PROPAGATING WAVES:

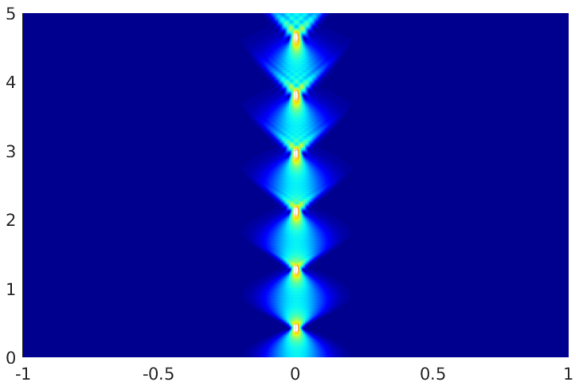

$x_0 = 0, \xi_0 = \pi$, mesh $\mathbf{g}^{\mathbf{h},\mathbf{1}}$

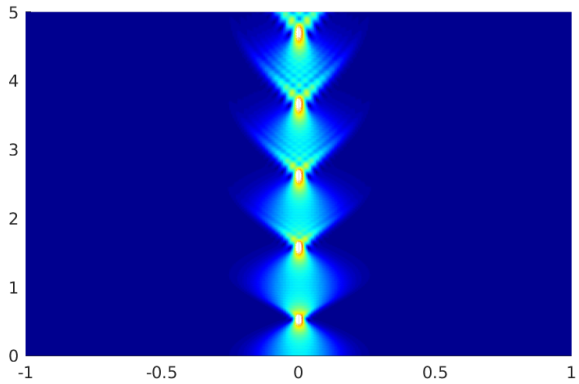

$x_0 = 0, \xi_0 = \pi$, mesh $\mathbf{g}^{\mathbf{h},\mathbf{2}}$

INTERNAL REFLECTION:

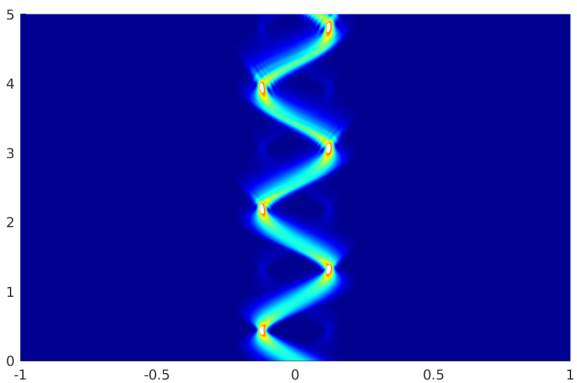

$x_0 = 0, \xi_0 = \frac{4\pi}{5}$, mesh $\mathbf{g}^{\mathbf{h},\mathbf{1}}$

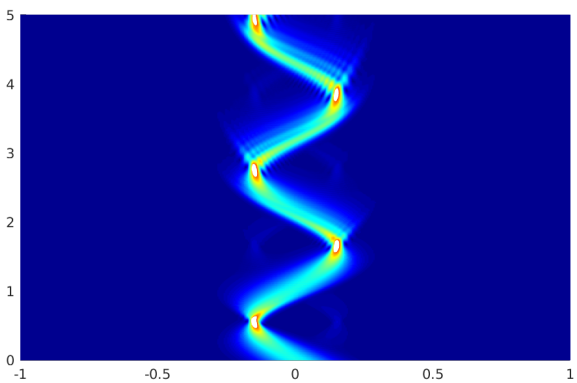

$x_0 = 0, \xi_0 = \frac{4\pi}{5}$, mesh $\mathbf{g}^{\mathbf{h},\mathbf{2}}$

Numerical example - forward Euler

- We have several different initial positions which, at frequency $\xi_0 = \pi$, generate non propagating waves.

x_0 = unstable equilibrium
$\xi_0 = \pi$, mesh $\mathbf{g}^{\mathbf{h},\mathbf{1}}$

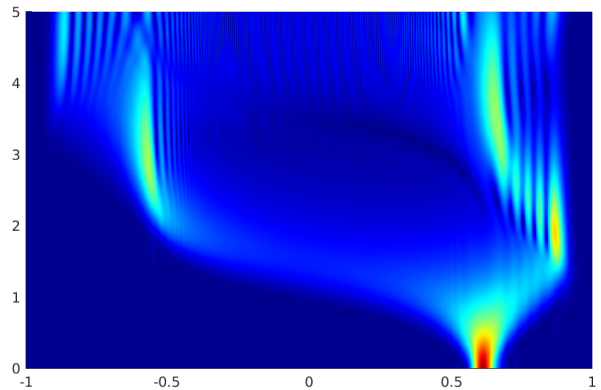

- Initial data corresponding to one of the unstable fixed point produce solutions that, apart from showing absence of propagation, present also a huge dispersion.
- These solutions, as soon as they move away from the unstable equilibrium point, are quite immediately affected by the orbits around the stable ones, thus generating the comeback effects that can be appreciated in the figure.

Two-dimensional wave equation

Two-dimensional wave equation

Two-dimensional wave equation

$$\begin{cases} \rho(\mathbf{z})\partial_t^2 u - div_{\mathbf{z}}\left(\sigma(\mathbf{z})\nabla_{\mathbf{z}} u\right) = 0, & (\mathbf{z}, t) \in \Omega \times (0, T) \\ u|_{\partial\Omega} = 0, & t \in (0, T) \\ u(\mathbf{z}, 0) = u^0(\mathbf{z}), \quad \partial_t u(\mathbf{z}, 0) = u^1(\mathbf{z}), & \mathbf{z} \in \Omega, \end{cases}$$

- $\mathbf{z} := (x, y)$
- $\Omega := (-1, 1)^2$
- $\rho, \sigma \in L^\infty(\Omega)$ with $\rho(\mathbf{z}) \geq \rho^* > 0$ and $\sigma(\mathbf{z}) \geq \sigma^* > 0$.

Semi-discrete approximation

Uniform mesh

$$\mathbf{G}^h := \Big\{ \mathbf{z}_{j,k} := (x_j, y_k) = (-1 + jh_x, -1 + kh_y), \\ j = 0, \dots, M+1, k = 0, \dots, N+1 \Big\}$$

Non-uniform mesh

g_1, g_2: diffeomorphisms of $\Omega \quad \Rightarrow \mathbf{G}^h_{\mathbf{g}} := \Big\{ \boldsymbol{\omega}_{j,k} := (v_j, \zeta_k) = (g_1(x_j), g_2(y_k)) \Big\}$

Hamiltonian system

Discrete Hamiltonian

$$\mathcal{P}(x, y, t, \xi, \eta, \tau) := \tau^2 - \Lambda(x, y, \xi, \eta)$$

$$\Lambda(x, y, \xi, \eta) := \frac{\sigma(x, y)}{\rho(x, y)} \left(4 \sin^2 \left(\frac{\xi}{2} \right) \frac{1}{g_1'(x)^2} + 4 \sin^2 \left(\frac{\eta}{2} \right) \frac{1}{g_2'(y)^2} \right).$$

Discrete bi-characteristic rays

$$\begin{cases} \dot{\mathbf{z}}_e(s) = \nabla_{\boldsymbol{\theta}_e} \mathcal{P}(\mathbf{z}_e(s), \boldsymbol{\theta}_e(s)), & \mathbf{z}_e(0) = \mathbf{z}_e^0 := (x_0, y_0, t_0) \\ \dot{t}(s) = 2\tau(s), & t(0) = 0 \\ \dot{\boldsymbol{\theta}}_e(s) = -\nabla_{\mathbf{z}_e} \mathcal{P}(\mathbf{z}_e(s), \boldsymbol{\theta}_e(s)), & \boldsymbol{\theta}_e(0) = \boldsymbol{\theta}_e^0 := (\xi_0, \eta_0, \tau_0) \\ \dot{\tau}(s) = 0, & \tau(0) = \tau_0. \end{cases}$$

$$\mathbf{z}_e := (x, y, t), \quad \boldsymbol{\theta}_e := (\xi, \eta, \tau)$$

Hamiltonian system

Assume $\rho = \sigma \equiv 1$.

HAMILTONIAN SYSTEM IN THE x COMPONENT:

$$\begin{cases} \dot{x}^{\pm}(t) = \mp \dfrac{r_1}{r_0} g_1'(g_1^{-1}(x^{\pm}(t)))\partial_\xi \lambda_1(g_1^{-1}(x^{\pm}(t)), \xi^{\pm}(t)) \\ \dot{\xi}^{\pm}(t) = \mp \dfrac{r_1}{r_0} \partial_x \lambda_1(g_1^{-1}(x^{\pm}(t)), \xi^{\pm}(t)) \end{cases}$$

HAMILTONIAN SYSTEM IN THE y COMPONENT:

$$\begin{cases} \dot{y}^{\pm}(t) = \mp \dfrac{r_2}{r_0} g_2'(g_2^{-1}(y^{\pm}(t)))\partial_\eta \lambda_2(g_2^{-1}(y^{\pm}(t)), \eta^{\pm}(t)) \\ \dot{\eta}^{\pm}(t) = \mp \dfrac{r_2}{r_0} \partial_y \lambda_2(g_2^{-1}(y^{\pm}(t)), \eta^{\pm}(t)). \end{cases}$$

- $r_0 := \sqrt{\Lambda(\mathbf{z}^{\pm}(t), \boldsymbol{\theta}^{\pm}(t))}$, $r_1 := \lambda_1(x^{\pm}(t), \xi^{\pm}(t))$, $r_2 := \lambda_2(y^{\pm}(t), \eta^{\pm}(t))$,
- $\lambda_1(x, \xi) := 2 \sin\left(\dfrac{\xi}{2}\right) \dfrac{1}{g_1'(x)}$, $\lambda_2(y, \eta) := 2 \sin\left(\dfrac{\eta}{2}\right) \dfrac{1}{g_2'(y)}$.

Mesh

MESH FUNCTIONS: $g_1(x) = g_2(x) = \tan\left(\frac{\pi}{4}x\right) =: g(x)$

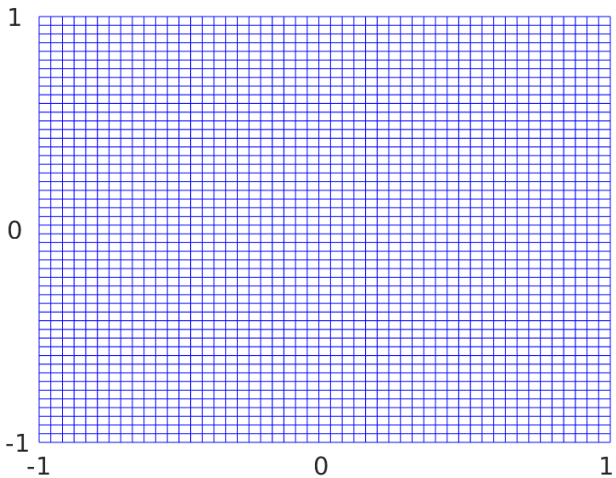

Uniform grid

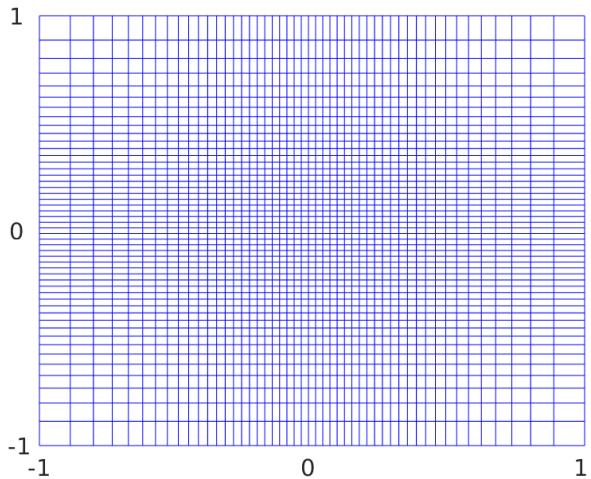

Non-uniform grid

Numerical solution

Solution in Fourier series

$$\mathbf{u^h} = \sum_{j=1}^{M}\sum_{k=1}^{N} \beta_{j,k}\Phi_{j,k}(\boldsymbol{\omega})\, e^{it\sqrt{\lambda_{j,k}}}.$$

- $\boldsymbol{\omega} := (v, \zeta)$
- $\{\Phi_{j,k}, \lambda_{j,k}\}$ are the eigenvector and the eigenvalues of the discrete Laplacian $-\Delta_{\boldsymbol{\omega}}$ on the refined mesh $\mathbf{G}^h_{\mathbf{g}}$

$$-\Delta_{\boldsymbol{\omega}}\Phi_{j,k} = \lambda_{j,k}\Phi_{j,k}, \quad j = 1, \ldots, M, \quad k = 1, \ldots, N.$$

- $\beta_{j,k}$: corresponding Fourier coefficients of the initial datum $\mathbf{u}^{0,\mathbf{h}}$.

INITIAL DATUM:

$$u^0(x,y) = \exp\left[-\gamma\left((x-x_0)^2 + (y-y_0)^2\right)\right]\exp\left[i\left(\frac{x\xi_0}{h} + \frac{y\eta_0}{h}\right)\right]$$

$$\gamma := h^{-0.9}.$$

Plots

At low frequencies, the solution remains concentrated and propagates along straight characteristics which reach the boundary, where there is reflection according to the Descartes-Snell's law. This independently on whether we use a uniform or a non-uniform mesh.

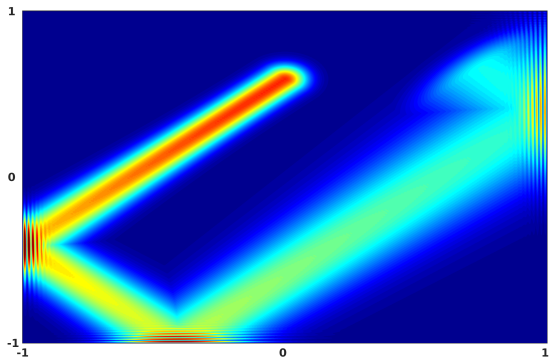

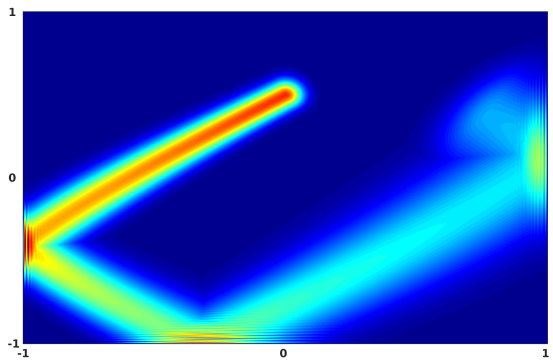

$(x_0, y_0, \xi_0, \eta_0) = (0, 1/2, \pi/4, \pi/4)$. The discretization is done on a uniform mesh (left) and on a non-uniform one obtained through the mesh function **g** (right).

High frequency pathologies

NON PROPAGATING WAVES:

- $(x_0, y_0, \xi_0, \eta_0) = (1, 0, \pi/2, \pi)$, uniform (left) and non-uniform (right) mesh

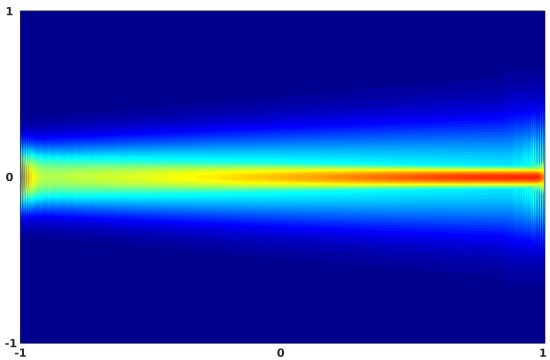

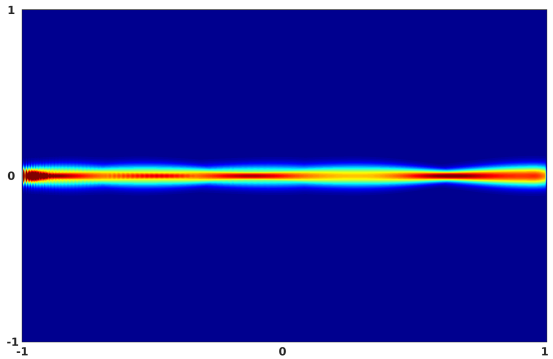

- $(x_0, y_0, \xi_0, \eta_0) = (0, 0, \pi, \pi)$, uniform (left) and non-uniform (right) mesh

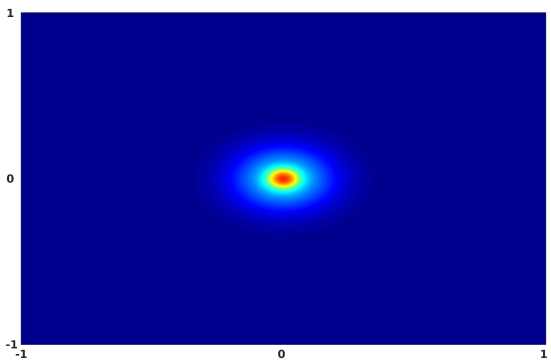

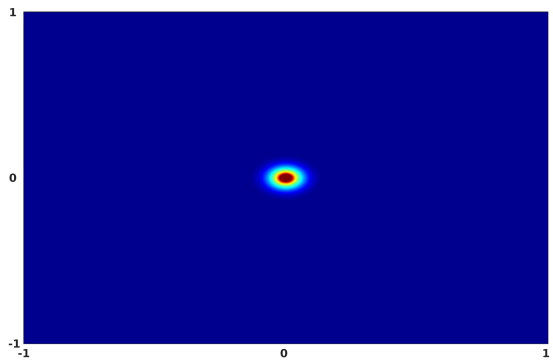

High frequency pathologies

JUSTIFICATION:

Hamiltonian system in the x/y direction

$$\begin{cases} \dot{x}(t) = -\dfrac{4}{r_0\pi}\sin(\xi(t))\dfrac{1}{x(t)^2+1} \\ \dot{\xi}(t) = -\dfrac{32}{r_0\pi}\sin^2\left(\dfrac{\xi(t)}{2}\right)\dfrac{x(t)}{(x(t)^2+1)^2} \end{cases} \qquad \begin{cases} \dot{y}(t) = -\dfrac{4}{r_0\pi}\sin(\eta(t))\dfrac{1}{y(t)^2+1} \\ \dot{\eta}(t) = -\dfrac{32}{r_0\pi}\sin^2\left(\dfrac{\eta(t)}{2}\right)\dfrac{y(t)}{(y(t)^2+1)^2}. \end{cases}$$

$P_e := (0,\pi)$: unique equilibrium for both systems.

- $(x_0, y_0, \xi_0, \eta_0) = (0, y_0, \pi, \eta_0)$: the corresponding solution does not propagates in the vertical direction.
- $(x_0, y_0, \xi_0, \eta_0) = (x_0, 0, \xi_0, \pi)$: the corresponding solution does not propagates in the horizontal direction.
- $(x_0, y_0, \xi_0, \eta_0) = (0, 0, \pi, \pi)$: the corresponding solution does not propagates neither in the vertical nor in the horizontal direction.

High frequency pathologies

INTERNAL REFLECTION:

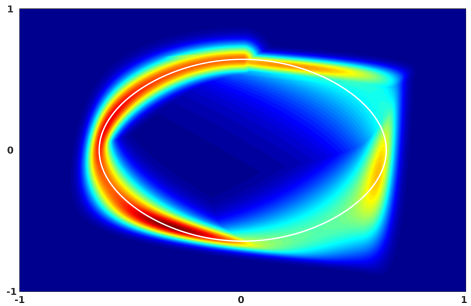

(a)

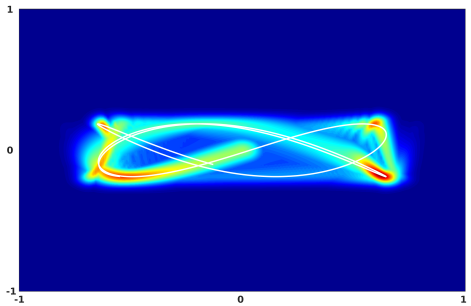

(b)

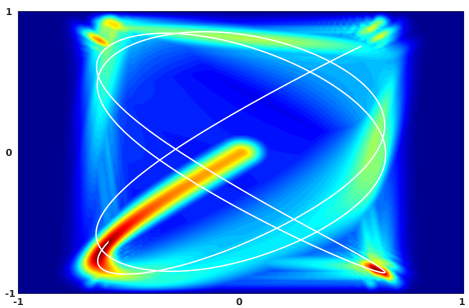

(c)

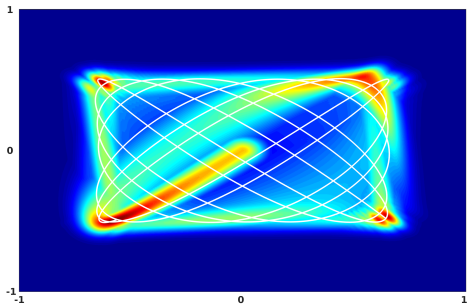

(d)

	x_0	y_0	ξ_0	η_0	T
Figure (a)	0	$\tan(\arccos(\sqrt[4]{1/2}))$	$\pi/2$	π	$8s$
Figure (b)	0	0	$\pi/2$	$5\pi/6$	$21s$
Figure (c)	0	0	$\pi/2$	$7\pi/18$	$37s$
Figure (d)	0	0	$\pi/2$	$7\pi/12$	$118s$

Numerical control of the wave equation

Motivations for the study presented

This study is motivated by **control theory** and **inverse problems**.

> Boundary controllability and identifiability properties of solutions of wave equations hold because of the fact that the energy is driven by characteristics that reach a sub-region of the domain or of its boundary where the controllers or observers are placed.

In the framework of wave-like processes, observability is guaranteed by the **geometric control condition** (GCC), requiring all rays of geometric optics to enter the control region during the control time.

C. Bardos, G. Lebeau and J. Rauch, SIAM J. Control Optim., 1992

L. Baudouin and S. Ervedoza, SIAM J. Control Optim., 2013

L. Baudouin, S. Ervedoza and A. Osses, J. Math. Pures Appl., 2015

Motivations for the study presented

When the wave equation is approximated by **finite difference methods**, observability/controllability may be lost under numerical discretization as the mesh size tends to zero, due to the existence of **high-frequency spurious solutions** for which the group velocity vanishes.

These high-frequency solutions are such that the energy concentrated in the control region is asymptotically smaller than the total energy, and we have **exponential blow-up** of the observability constant as $h \to 0$.

This is related with the explicit form of the discrete spectrum of the FD Laplacian and with the **lack of asymptotic spectral gap**.

Discrete spectrum

$$\lambda_k^h = \frac{4}{h^2} \sin^2\left(\frac{k\pi h}{2}\right) \to \lambda_k = k^2\pi^2, \quad \text{as } h \to 0^+$$

E. Zuazua, *Propagation, observation, control and numerical approximation of waves*, SIAM Rev., 2015.

Motivations for the study presented

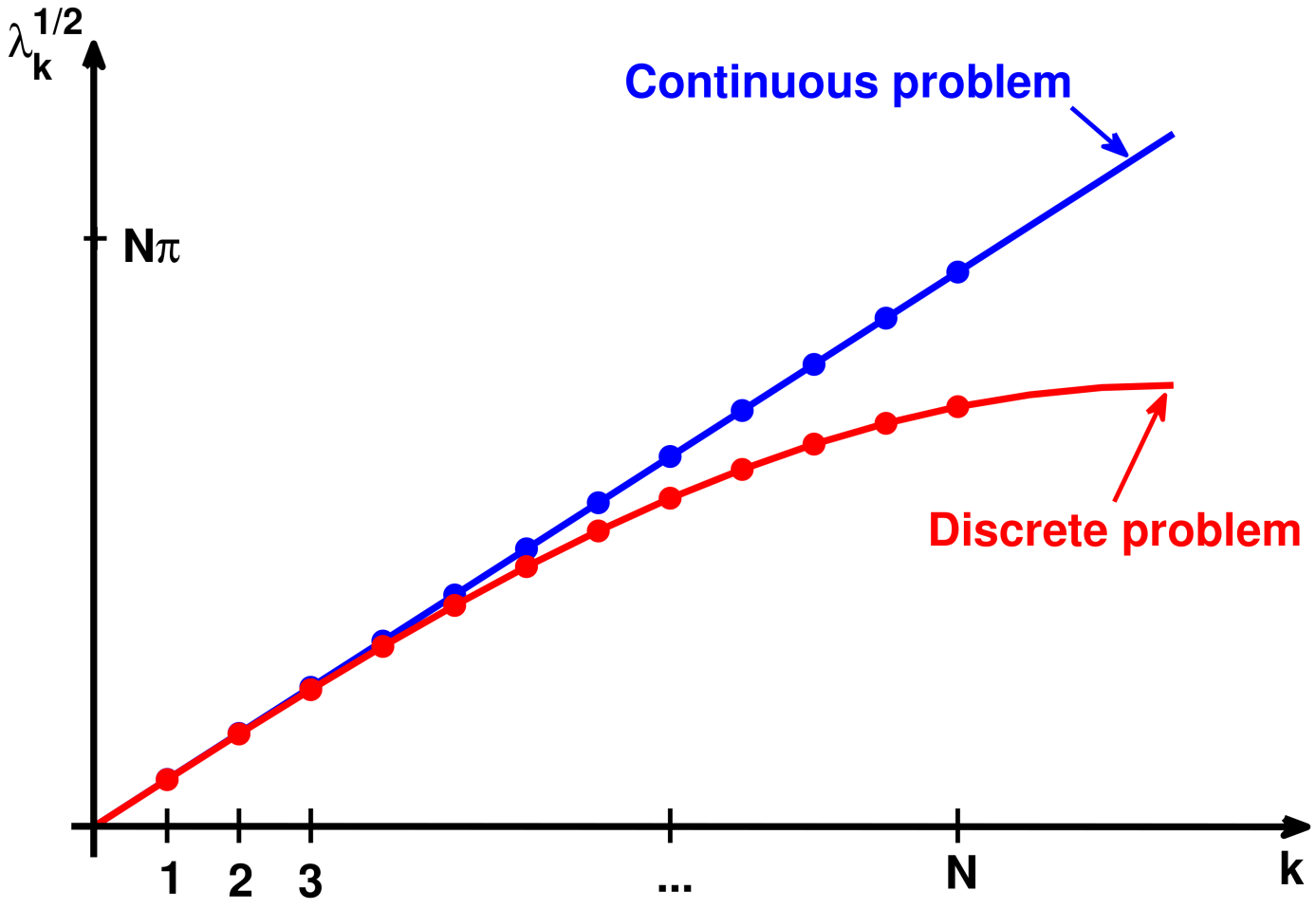

Possible remedies

FOURIER FILTERING:

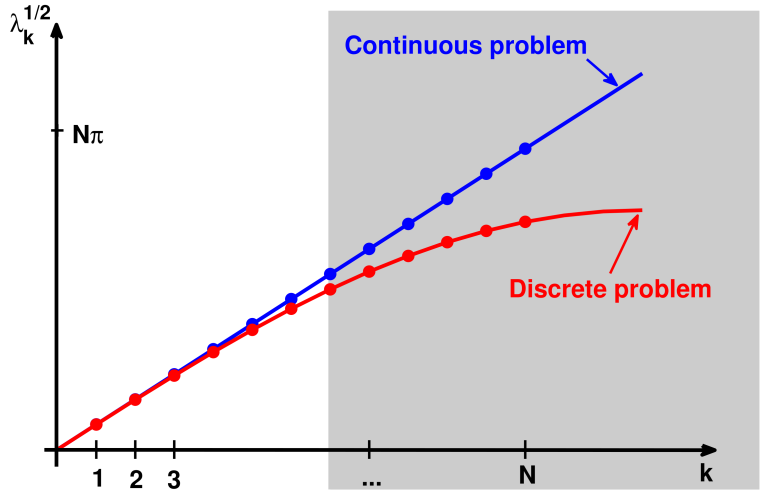

Discrete spectrum

To filter the high frequencies, keeping the components $k \leq \delta/h$ with $0 < \delta < 1$. Then the group velocity remains uniformly bounded below and uniform observation holds in time $T(\delta) > 2$ such that $T(\delta) \to 2$ as $\delta \to 0$.

S. Ervedoza and E. Zuazua, *The wave equation: control and numerics*, in Control and stabilization of PDEs, Springer, 2012.

Possible remedies

TWO-GRID ALGORITHMS:

High frequencies producing lack of gap and spurious numerical solutions correspond to large eigenvalues

$$\sqrt{\lambda_k^h} \sim \frac{2}{h}$$

When refining the mesh

$$h \mapsto \frac{h}{2} \quad \to \quad \sqrt{\lambda_k^{h/2}} \sim \frac{4}{h}$$

Refining the mesh $h \mapsto \frac{h}{2}$ produces the same effect as filtering with parameter $1/2$.

Two-grid algorithms

Compute solutions of the wave equation on a fine grid of size h, starting from slowly oscillating initial data discretized on a coarse mesh of size $2h$. These solutions **are no longer pathological**.

L. Ignat and E. Zuazua, *Convergence of a two-grid algorithm for the control of the wave equation*, JEMS, 2009.

Possible remedies

OTHER POSSIBLE REMEDIES:

- **Tikhonov regularization**: reinforce the observation operator by adding an extra observation, distributed everywhere in the discrete grid, so that observability holds uniformly on the mesh-size parameter h for all solutions.

  R. Glowinski, C. H. Li and J.-L. Lions, *A numerical approach to the exact boundary controllability of the wave equation*, Japan J. Appl. Math., 1990.

- **Employ mixed FE**: using a mixed FE scheme for the space discretization of the wave equation may allow recovering the spectral gap. C. Castro and S. Micu,

  Boundary controllability of a linear semi-discrete 1d wave equation derived from a mixed finite element method, Numer. Math., 2006.

- **Use non-uniform meshes**: discretizing on appropriately built non-uniform meshes may remove the high-frequency pathologies. S. Ervedoza, A. Marica and E. Zuazua,

  Numerical meshes ensuring uniform observability of one-dimensional waves: construction and analysis, IMA J. Numer. Anal., 2015.

THANK YOU FOR YOUR ATTENTION!

Funding

- European Research Council (ERC): grant agreements NO: 694126-DyCon and No.765579-ConFlex.
- MINECO (Spain): Grant PID2020-112617GB-C22 KILEARN
- Alexander von Humboldt-Professorship program
- DFG (Germany): Transregio 154 Project "Mathematical Modelling,Simulation and Optimization Using the Example of Gas Networks"
- COST Action grant CA18232, "Mathematical models for interacting dynamics on networks".